This article was published in

Seppälä A, Lampinen MJ. 2004. On the non-linearity of osmotic flow. Experimental Thermal and Fluid Science 28: 283-296.

Available online at www.sciencedirect.com
SCIENCE DIRECT®
Experimental Thermal and Fluid Science 28 (2004) 283–296
Experimental Thermal and Fluid Science
www.elsevier.com/locate/etfs

On the non-linearity of osmotic flow

Ari Seppälä *, Markku J. Lampinen

Laboratory of Applied Thermodynamics, Department of Mechanical Engineering, Helsinki University of Technology, P.O. Box 4100, FIN-02015 HUT, Finland

Received 28 November 2002; accepted 28 May 2003

Abstract

The osmotic water flow and the solute flow through three different commercial cellulose acetate membranes were measured with different NaCl concentrations, hydrostatic pressures and module flow conditions. Based on the measurements, the concentrations on the surfaces of the selective layer of the membrane were theoretically calculated and the results applied to fit equations whose derivation is based on the theory of dimensional analysis. The results show that the frequently used linear forms of the osmotic transport equation do not satisfactorily describe the phenomenon. The proposed forms of a new transport equation for water flux are $\frac{A_w \Delta x_s - B_w \Delta p_r}{1+\Phi \bar{x}_s}$ or $A_w \Delta\sqrt{x_s} - B_w \Delta\sqrt{p_r}$ where A_w, B_w and Φ are the transport coefficients, x_s is the molar fraction of the solute, $\bar{x}_s$ is the mean molar fraction and p_r is the dimensionless pressure. The question of whether the non-linear phenomenon of osmotic water transport is much more general than hitherto expected, is raised. Criticism is provided on the assumption of internal concentration polarisation as an explanation of the apparent non-linearities appearing in the experiments. The two-coefficient linear equation was found sufficient to describe the measured solute flux. The one-coefficient linear equation for solute flux, relating the flux only to the solute concentration difference or molar fraction difference, was found to be inadequate.

Keywords: Osmosis; Transport equation; Dimensional analysis

1. Introduction

In osmosis, two solutions of different composition are separated from each other by a selective membrane. The membrane allows water or some other solvent to penetrate through at a considerably higher rate than the solute. Osmosis makes possible the natural transport of solvent from a low pressure solution to a high pressure solution where the solute concentration is sufficiently high. Osmosis is a very common phenomenon in biological systems, but it has also potential for technical applications due to the possibility to transport fluid against the pressure gradient and due to the possibility to create large forces or pressures. The most studied technical application is the energy production from salinity differences of ocean and river water (see e.g. [1]).

In studies of osmosis, the transport for different species is repeatedly estimated by a linear relationship with concentration (or osmotic potential/pressure) difference and hydrostatic pressure difference. However, in osmotic experiments, for example with biological membranes [2–9] and industrial membranes [10–12], the osmotic water flow has been found to change non-linearly especially in respect to the changes on the concentration difference between the bulk solutions (the apparent behaviour). This non-linear performance is often suggested to be caused by the concentration boundary layers in fluids adjacent to the membrane, by solute accumulation (often called the internal polarisation) inside the porous support structure of the membrane [11,13], or by the mutual effect of several serial membranes (e.g. [14]). It has frequently been assumed that when all concentration boundary layers have been correctly accounted for, the true response (of the actual selective layer of the membrane) to increasing solute concentration and pressure would be linear. Only a very small number of authors have pointed out the possibility

* Corresponding author. Fax: +358-9-451-3419.
E-mail address: ari.seppala@hut.fi (A. Seppälä).

0894-1777/$ - see front matter © 2003 Elsevier Inc. All rights reserved.
doi:10.1016/j.expthermflusci.2003.10.001

Nomenclature

A_w, B_w	transport coefficients for water flow, mol/m^2 s
A_s, B_s	transport coefficients for solute flow, mol/m^2 s
c	total concentration of solution, mol/m^3 or 1/m^3
c_H	(initial) bulk solute ion concentration of the high-concentration solution, mol/m^3
c_L	(initial) bulk solute ion concentration of the low-concentration solution, mol/m^3
c_s	solute ion concentration, mol/m^3 or 1/m^3
c_s^0	initial solute ion concentration at channel (either c_H or c_L), mol/m^3
D	diffusion coefficient, m^2/s, we used $D = 1.5 \times 10^{-9}$ m^2/s for NaCl water solution
D_{eff}	effective diffusion coefficient, m^2/s
F_i	free energy of the interface, J
g	gravitational acceleration, m/s^2
h	channel height, m
J	molar flux of solute or solvent, mol/m^2 s or 1/m^2 s
J_s	molar flux of solute ions, mol/m^2 s or 1/m^2 s
J_w	molar flux of water, mol/m^2 s or 1/m^2 s
k_B	gas constant, N m/K
k_p	permeability, m^2
L	length, m
M	molar mass, kg/mol
p	hydrostatic pressure, Pa or bar
p_r	dimensionless pressure
$\Re$	universal gas constant, J/mol K
R_f	resistance for flow, N s
R_{diff}	diffusion resistance, m^{-1} s
Re_w	wall Reynolds number, dimensionless
T	temperature, K or °C
u	velocity of the solution inside the channel, tangential to the membrane, m/s
u_{slip}	tangential (slip) velocity on the surface of porous matter, m/s
u_m	tangential mean velocity at cross-sectional area of channel, m/s
v	velocity of the solution inside the channel, normal to the membrane, m/s
v_w	osmotic total flux through the membrane, m^3/m^2 s
W	channel width, m
x	co-ordinate, tangential to the membrane surface, m
x_s	mole fraction of solute (ions), dimensionless
y	co-ordinate, normal to the membrane surface, m
α	coefficient of slip coefficient, dimensionless
Γ	driving force of flows, N/m^2
λ	dimensionless co-ordinate ($= y/h$)
μ	dynamic viscosity, N s/m^2
ν	kinematic viscosity, m^2/s
π	osmotic potential (osmotic pressure), bar or 3.14159...
Π	dimensionless term
τ	tortuosity, dimensionless
Φ	transport coefficient, dimensionless
Ω	dynamical osmotic potential, N/m^2
$\varnothing$	porosity, dimensionless
∂	partial differential
Θ	dimensionless slip coefficient

that the phenomenon itself could be non-linear. Some of these authors have proposed, but not proved, reasons for this non-linearity. Massaldi and Borzi [15] suggested that phenomena such as cavitation and partial clogging could explain the non-linearities. Fuls et al. [16] suggested instead that the membrane could compact not only as a result of the pressure applied, but also because of the osmotic potential causing a reduction in the membrane's permeability.

In this study a laboratory cross-flow osmosis module for flat sheet membranes was constructed and applied to measure the steady-state transport of species through three different commercial cellulose acetate membranes. Based on these measurements, the concentrations on both sides of the selective layer of the membranes were theoretically calculated and then used to analyse different forms of transport equations.

2. Experimental methods

2.1. Apparatus

The experimental facility is shown in Fig. 1. The low-concentration solution (lcs) is pumped from a container into the lcs part of the osmotic module. The module is manufactured from a transparent material. Most of the lcs ends up in an outlet container, while a small fraction of the water penetrates, due to osmosis, through the membrane into the high-concentration solution (hcs). The electric conductivity of the outlet container is measured during the experiments. The increase in solute of lcs is determined from this measurement and then the solute flux through the membrane is estimated. The lcs flow can be pressurised by throttling the flow with a valve.

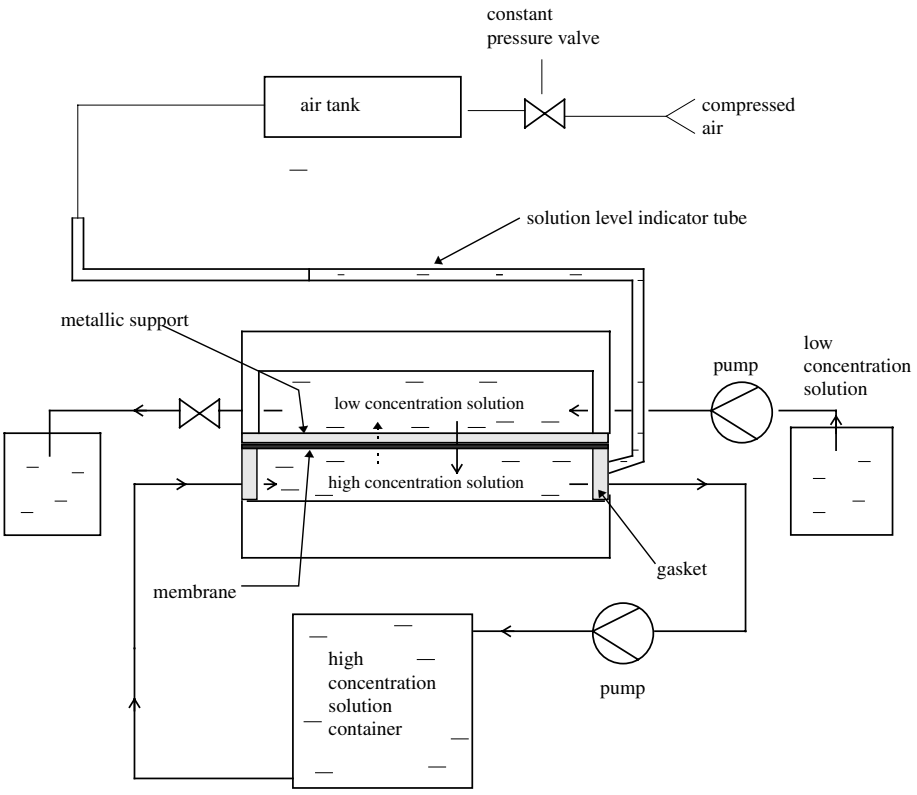

Fig. 1. Experimental apparatus [10].

The hcs is pumped from a container into the hcs part of the module in the opposite direction to the lcs (counter-flow). The hcs flows inside the module in a space that is enveloped by an elastic gasket. The volume of the hcs part of the module depends, then, on the force applied to press the lcs and hcs side modules together.

For steady-state measurements, the change in the hcs liquid volume, and thus the total permeating flow to the hcs side, can be measured from the change in the liquid level on the horizontal indicator tube that is linked to the hcs side. The hcs is pressurised, via this tube, by compressed air. The hcs is recycled from the module back to the container. The volume of the hcs container is so large that the effect of the dilution of the hcs is meaningless during the tests. The weights of both lcs containers were measured during the experiments to check the water balance; in a stationary state the difference between measured inlet and outlet flows of the lcs should be equal to the osmotic flow measured in the indicator tube.

The lcs side of the module consists of four equal channels, 0.95 cm wide, 1 mm in height and 8 cm long. The metallic support, which provides additional mechanical support to the membrane, is covered at the ends by an insulator so that the entrance and exit conditions of the module will not affect hydrodynamic conditions (when the boundary layers are calculated) at the positions where osmosis occurs. Thus, osmotic flow occurs only in the middle section of the module, its length being 3.6 cm.

The lcs and hcs were produced by adding an appropriate amount of NaCl in degassed low ion-concentration water solution. When NaCl is not added, this solution consists of several dissolved ions, the total ionic concentration being 1.4 mol/m^3.

2.2. Membranes and support structures

Three flat sheet asymmetric cellulose acetate membranes were tested: the Osmonics Inc. SS10 and ST10 and the Fluid Systems CTA-HR membrane. The studied membranes, as well as many biological membranes, consist of a very thin selective layer (skin) and of a thick porous substructure. The actual osmotic phenomenon is customarily assumed to occur only at the skin. The purpose of the substructure is to give mechanical support to the skin.

The dry and wet weights of the membranes were measured, and from these measurements the overall porosity of the support structure of each membrane was determined. For a more detailed analysis, the support structure of each membrane was divided into 2–3 sublayers. The porosity and tortuosity of each sublayer was additionally estimated by the Monte-Carlo method from

Table 1
Estimated properties of metallic support and the porous substructure

Structure	Thickness, Δy (μm)	Porosity, $\varnothing$	Tortuosity, τ	Estimated (Eq. (A.15)) resistance, R_{diff} (s/m)
Metallic support	540	0.53	1.05	713 000
SS10				
Porous substructures				
-Layer 1	100	0.39	1.6	274 000
-Layer 2	52	0.28	2.1	260 000
-Layer 3	8	0.36	3.3	49 000
Total	160			583 000
ST10				
Porous substructures				
-Layer 1	110	0.40	1.6	294 000
-Layer 2	50	0.40	2.9	242 000
Total	160			536 000
CTA				
Porous substructures				
-Layer 1	120	0.40	1.6	320 000
-Layer 2	50	0.33	2.8	283 000
Total	170			603 000

$D = 1.5 \times 10^{-9}$ m^2/s.

SEM pictures. Relatively large errors may occur in tortuosity values for layers 2 and 3. The porosity and the tortuosity values (presented in Table 1) are needed for estimation of the diffusion resistance of the support structure R_{diff} (defined in Eq. (A.15) in Appendix A.3). We will later confirm our conclusions by estimating the results with various values of R_{diff}. The holes of the additional metallic support were so large that the porosity and tortuosity was accurately estimated from the geometry of the structure.

3. Calculation of the concentration on the surfaces of the selective layer

To study the transport equations for the skin we first need to estimate the concentrations at the surfaces of the skin. Therefore, we have calculated, by utilising the measured data, the concentration profiles (illustrated in Fig. 2) in the adjacent solutions, inside the metallic support, and inside the porous support structure of the membrane. It is approximated that the hydrostatic pressure (p) remains constant throughout the support structures. To determine the concentrations c_{s1} and c_{s4}, we have numerically solved, by means of the control volume method, a two-dimensional steady-state continuity equation for solute inside the module channels (see Appendix A.1). The determination of the solution velocity and pressure distributions inside the channels is explained in more detail in Appendix A.2. The four channels of the lcs side are assumed to be under equal conditions. The resulting distributions of solute concentration on the surfaces of the skin and on the surface of the metallic support are then averaged in space. The average value of c_{s1} is then applied to determine the one-dimensional concentration distribution inside the support and substructures (Appendix A.3), and finally to estimate the solute concentration at the reverse side of the skin (c_{s3}).

4. Dimensional analysis of the transport equations for the selective layer

We assume that the fluxes (J) of the solute and solvent through the selective layer of the membrane can be expressed in the form

$$J = \frac{\Gamma}{R_f} \tag{1}$$

where Γ is the driving force for the fluxes, and R_f the resistance for the fluxes. We will try to find the forms of the Γ and R_f by the theory of dimensional analysis. All the variables are expressed in basic units of force [F], length [L], time [T] and temperature [θ]. J is expressed in the number of molecules or ions penetrating a cross-sectional area in time. The unit of J is [$L^{-2}T^{-1}$], Γ is expressed in [FL^{-2}] and R_f in [FT].

We derived two different expressions for the driving force Γ. First, we found the expression for the driving force which is assumed to depend on the pressure difference Δp [FL^{-2}], the concentration difference of the solute Δc_s [L^{-3}], the total concentration of the solution c [L^{-3}], the absolute temperature T [θ] and a gas constant k_B [$FL\theta^{-1}$]. Thus

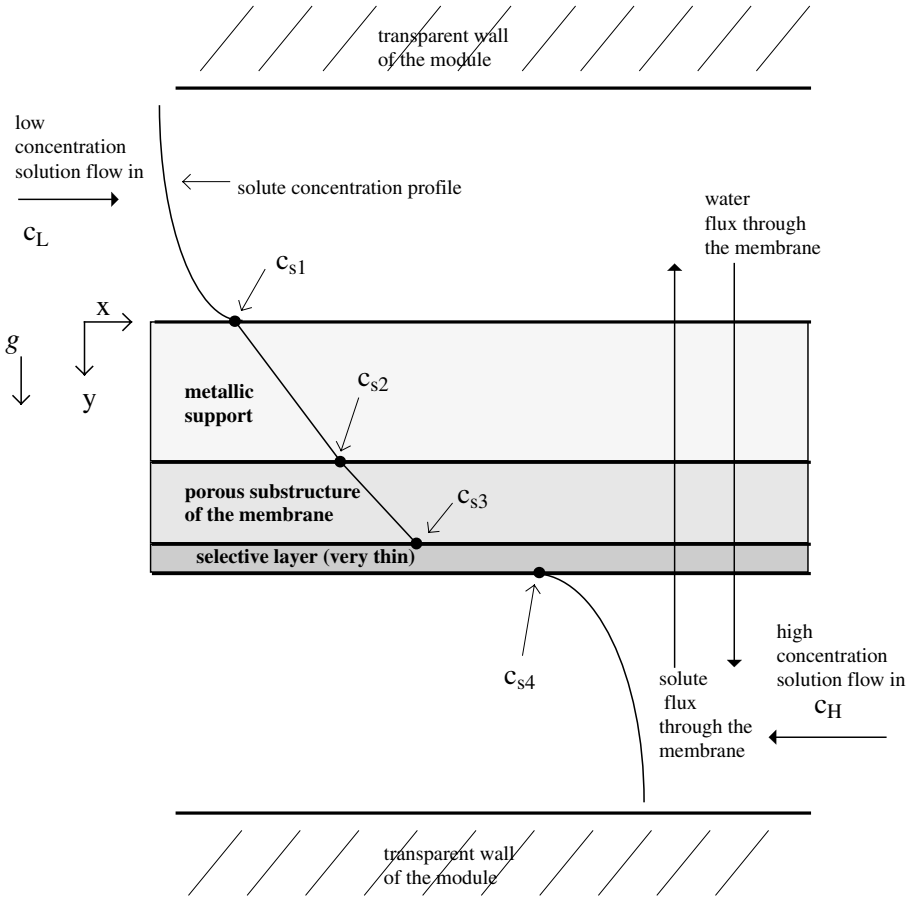

Fig. 2. Concentration distribution inside channels, support- and substructures ($C_H > C_{s4} > C_{s3} > C_{s3} > C_{s2} > C_{s1} > C_L$, g = gravitational acceleration). The real thickness of the selective layer is considerably smaller than illustrated in figure.

$$\Gamma = \Gamma(\Delta p, \Delta c_s, c, T, k_B) \tag{2}$$

The gas constant k_B is interpreted as being equal with Boltzmann's constant if a gas in equilibrium with the liquid solution under study is considered as an ideal gas. However, k_B deviates from Boltzmann's constant if the gas in equilibrium with the solution being considered is a real gas. Therefore, if the pressure and temperature of the solution are at such a level that gas in equilibrium with it had to be handled as real gas, then k_B is an appropriate transformation of Boltzmann's constant (Boltzmann's constant multiplied with a non-dimensional parameter). We now have six variables (Γ, Δp, Δc_s, c, T, k_B), which consists in basic units F, L and θ, in the model of Eq. (2). According to Buckingham's theorem (see e.g. [19]) the number of variables can be reduced from six to three dimensionless Π-variables (the number of variables minus the number of basic units equals to the number of dimensionless variables). That is, the problem can be stated as $\Pi_1 = Q_1(\Pi_2, \Pi_3)$, where Q_1 is a function to be found experimentally. The following dimensionless terms can be found:

$$\Pi_1 = \frac{\Gamma}{ck_BT}, \quad \Pi_2 = \frac{\Delta c_s}{c}, \quad \Pi_3 = \frac{\Delta p}{ck_BT}$$

Thus, the driving force is

$$\Gamma = ck_BT \cdot Q_1(\Pi_2, \Pi_3) \tag{3}$$

In the second model for the driving force we assume there to appear a dynamic osmotic potential Ω [FL^{-2}] (deviating from the equilibrium osmotic potential, i.e. from the osmotic pressure). The driving force arises from the difference between the potential values on the surfaces of the selective layer. The flow is then expressed as

$$J = \frac{\Delta\Omega}{R_f} \tag{4}$$

The derivation of the expression for dynamic osmotic potential is straightforwardly the same as the previous derivation of the driving force Γ, except that the concentration difference is changed to the actual concentration at the surface and the pressure difference to the actual value of the pressure at the surface. The expression for the potential is thus

$$\Omega = ck_{\mathrm{B}}T \cdot Q_2(\Pi_4, \Pi_5) \tag{5}$$

where $\Pi_4 = c_{\mathrm{s}}/c$, $\Pi_5 = p/ck_{\mathrm{B}}T$.

Next, the expression for the resistance to the flow R_{f} [FT] is sought. We assume that it depends on the diffusion resistance R_{diff} [$\mathrm{L}^{-1}\mathrm{T}$] between the solute and solvent, the dynamic viscosity of the solution μ [$\mathrm{FL}^{-2}\mathrm{T}$], the average total concentration of the solution inside the selective layer $\bar{c}$ [L^{-3}], the average concentration of the solute inside the membrane $\bar{c}_{\mathrm{s}}$ [L^{-3}] and on the free energy of the interface between the solid and fluid phase F_{i} [FL]. We have now six variables and three basic dimensions (F,L,T) in the model for finding the expression $R_{\mathrm{f}} = R_{\mathrm{f}}(\mu, \bar{c}_{\mathrm{s}}, \bar{c}, F_{\mathrm{i}}, R_{\mathrm{diff}})$. This problem can be transformed into a problem expressed with three dimensionless variables

$$\Pi_6 = Q_3(\Pi_7, \Pi_8)$$

The following dimensionless terms can be found:

$$\Pi_6 = \frac{R_{\mathrm{f}}^3 \bar{c}^2}{\mu^3}, \quad \Pi_7 = \frac{\bar{c}_{\mathrm{s}}}{\bar{c}}, \quad \Pi_8 = \frac{R_{\mathrm{diff}}^3 F_{\mathrm{i}}^3 \bar{c}^2}{\mu^3}$$

Then the resistance is

$$R_{\mathrm{f}} = \frac{\mu}{\bar{c}^{2/3}} \cdot Q_3(\Pi_7, \Pi_8) \tag{6}$$

Inserting Eqs. (3) and (6) into Eq. (1), Model 1 for flows is

$$J = \frac{ck_{\mathrm{B}}T \cdot Q_1(\Pi_2, \Pi_3)}{\frac{\mu}{\bar{c}^{2/3}} \cdot Q_3(\Pi_7, \Pi_8)} \tag{7}$$

and inserting Eqs. (5) and (6) into Eq. (4), Model 2 is

$$J = \frac{\Delta[ck_{\mathrm{B}}T \cdot Q_2(\Pi_4, \Pi_5)]}{\frac{\mu}{\bar{c}^{2/3}} \cdot Q_3(\Pi_7, \Pi_8)} \tag{8}$$

The above two expressions are the most general forms of the transport equation of this study. The dimensionless variables are denoted as: $\Pi_2 = \Delta x_{\mathrm{s}}$ (molar fraction difference), $\Pi_3 = \Delta p_{\mathrm{r}}$ (dimensionless pressure difference), $\Pi_4 = x_{\mathrm{s}}$ (molar fraction), $\Pi_5 = p_{\mathrm{r}}$ (dimensionless pressure), $\Pi_7 = \bar{x}_{\mathrm{s}}$ (average molar fraction inside the selective layer). The unknown functions Q_1, Q_2 and Q_3 cannot be found by applying the theory of dimensional analysis. Therefore, we shall now model them with the following test functions

$$Q_1 = \pm A_1(\Pi_2)^k - A_2(\Pi_3)^n \tag{9}$$

$$Q_2 = \pm A_3(\Pi_4)^k - A_4(\Pi_5)^n \tag{10}$$

and

$$Q_3 = A_5\Pi_7 + A_6\Pi_8 \tag{11}$$

where $A_1, A_2, \ldots, A_6$ are constants. The plus sign in the first group of terms of the right-hand side of Eqs. (9) and (10) will be used for the water flux and the minus sign for the solute flux. For the purposes of the present study it is sufficient to keep the variables c, $k_{\mathrm{B}}T$, $\bar{c}$, F_{i}, R_{diff} and μ appearing in Π_1, Π_6 and Π_8 as constants, that is we include them into the transport coefficients. Substituting the test functions Q_1, Q_2 and Q_3 into Eqs. (7) and (8) results in

$$J = \frac{\pm A(\Delta x_{\mathrm{s}})^k - B(\Delta p_{\mathrm{r}})^n}{1 + \Phi\bar{x}_{\mathrm{s}}} \tag{12}$$

$$J = \frac{\pm A\,\Delta(x_{\mathrm{s}}^k) - B\,\Delta(p_{\mathrm{r}}^n)}{1 + \Phi\bar{x}_{\mathrm{s}}} \tag{13}$$

where A, B and Φ are understood to be transport coefficients which depend on the membrane and solution characteristics. By applying Boltzmann's constant as k_{B}, the dimensionless pressure can be expressed as

$$p_{\mathrm{r}} = \frac{p}{c\Re T} \tag{14}$$

where c is now in units $\mathrm{mol/m^3}$ and $\Re$ (J/mol K) is the universal gas constant.

The water flux (J_{w}) was studied in two special cases of Eqs. (12) and (13). First, the coefficient Φ is assumed to be 0. Then, the possible non-linearity is caused from the non-linearity of the driving force. The equations for water flux are then

$$J_{\mathrm{w}} = A_{\mathrm{w}}(\Delta x_{\mathrm{s}})^k - B_{\mathrm{w}}(\Delta p_{\mathrm{r}})^n \tag{15}$$

and

$$J_{\mathrm{w}} = A_{\mathrm{w}}\,\Delta(x_{\mathrm{s}}^k) - B_{\mathrm{w}}\,\Delta(p_{\mathrm{r}}^n) \tag{16}$$

A third water flux equation is achieved when the powers k and n in Eqs. (12) and (13) are assumed to be unity; then both equations result in

$$J_{\mathrm{w}} = \frac{A_{\mathrm{w}}\,\Delta x_{\mathrm{s}} - B_{\mathrm{w}}\,\Delta p_{\mathrm{r}}}{1 + \Phi\bar{x}_{\mathrm{s}}} \tag{17}$$

The possible non-linearity is caused in this case by the non-constant resistance. In Eq. (17), $\bar{x}_{\mathrm{s}}$ is taken in this study as $\bar{x}_{\mathrm{s}} = \frac{x_{\mathrm{s}4} + x_{\mathrm{s}3}}{2}$. Substituting Eq. (11) into Eq. (6), the total resistance can be written as

$$R_{\mathrm{f}} = A_5 R_{\mathrm{diff}} F_{\mathrm{i}} \bar{x}_{\mathrm{s}} + \frac{A_6\mu^3}{R_{\mathrm{diff}}^2 F_{\mathrm{i}}^2 \bar{c}^2}$$

One can show that this equation for the resistance results in an extremum value (minimum if $A_6 > 0$, maximum if $A_6 < 0$) in respect to term $R_{\mathrm{diff}}F_{\mathrm{i}}$ when

$$R_{\mathrm{diff}}F_{\mathrm{i}} = \frac{2A_6\mu^3}{A_5\bar{c}^2\bar{x}_{\mathrm{s}}}$$

The solute flux equation will be studied only for the case when the resistance is constant. This means that $\Phi = 0$ in Eqs. (12) and (13). The models for the solute flux equation are

$$J_{\mathrm{s}} = -[A_{\mathrm{s}}(\Delta x_{\mathrm{s}})^k + B_{\mathrm{s}}(\Delta p_{\mathrm{r}})^n] \tag{18}$$

and

$$J_{\mathrm{s}} = -[A_{\mathrm{s}}\,\Delta(x_{\mathrm{s}}^k) + B_{\mathrm{s}}\,\Delta(p_{\mathrm{r}}^n)] \tag{19}$$

5. Results

5.1. Experiments

A set of experiments was performed, with varying NaCl solution concentration and pressure on both sides of the membranes. In osmosis experiments, the concentration of the lcs varied within 0–1 wt.% and concentration of the hcs approximately within 1–5 wt.% for SS10 and ST10 membranes and within 3–10 wt.% for CTA-HR membrane. The experiments were performed until the steady state was found. The time needed for the experiments varied from 3 to 35 h. The pumping rates of pumps and flow height at the hcs side were also varied between the experiments, so that the results should not depend on particular hydrodynamic conditions in the module. The steady-state results of the experiments are shown in Table 2. The solute concentration, molar fraction and solute flux are given in this paper for the total number of dissolved ions ($Na^+ + Cl^-$). The measured total volume flow per membrane surface area, i.e. the osmotic flux (v_w), can be closely approximated as a water flux as the solute flux is, in all cases, considerably smaller than the water flux. Two of the experiments resulted in reverse osmosis, as can been seen from the minus sign of the total volume (osmotic) flux in Table 2. The temperatures during the experiments on the SS10, ST10 and CTA membranes were 23 ± 1, 26 ± 1 and 24.5 ± 0.5 °C, respectively.

Eight experiments were repeated: CTA-1, CTA-2, CTA-4 and SS10-1 once each and SS10-6 and SS10-7 both twice. The relative differences between the repeated experiments (measured solute and osmotic flux) were between 2% and 25%. The conclusion is that any transport equation estimating the fluxes should not give values that differ over 25% when compared to the measured values of the actual experiments.

The pressure changes inside the module channels were calculated according to the theory presented in [23]. It was confirmed that in all experiments these pressure differences parallel and perpendicular to the membrane were meaningless (below 15 Pa). The flows inside the module channels were, in all cases, laminar and the maximum wall Reynolds number in the experiments was $Re_w = 0.0012$ (see Appendix A.2). This causes only a very small error for first-order perturbation approximation [23]. Therefore, the requirements imposed by the perturbation treatment for derivation of the velocity and pressure profiles inside the module channels will be fulfilled.

Table 2
Experimental results for the osmotic flux (v_w) and the salt flux (J_s)

Membrane/ exp. no.	P_H (bar)	p_L (bar)	c_H (mol/m^3)	c_L (mol/m^3)	$\dot{V}_H \times 10^9$ (m^3/s)	$\dot{V}_L \times 10^9$ (m^3/s)	$h \times 10^4$ (m)	$v_w \times 10^7$ (m^3/m^2 s)	$J_S \times 10^5$ (mol/m^2 s)
SS10-1	1.6	1.0	342	1.4	383	39	11.4	4.91	−2.34
SS10-2	4.5	1.0	1020	1.4	186	11	5.1	4.91	−6.57
SS10-3	2.5	1.5	1020	1.4	110	28	11.4	8.53	−4.00
SS10-4	4.22	1.0	342	1.4	262	48	5.6	1.58	−4.53
SS10-5	6.6	1.0	1517	1.4	148	69	5.2	5.81	−11.7
SS10-6	4.1	1.0	1517	342	300	67	7.3	3.06	−8.68
SS10-7	3.1	1.0	683	1.4	186	115	7.2	6.19	−5.21
SS10-8	2.1	1.0	1517	1.4	34	20	11.4	8.30	−5.46
SS10-9	6.6	1.0	167	1.4	338	13	4.8	−8.30	−3.63
CTA-1	1.25	1.0	1517	1.4	110	23.5	11.4	2.34	−14.7
CTA-2	2	1.0	2007	1.4	186	20.1	11.4	1.96	−22.6
CTA-3	2.05	1.0	2007	342	338	21.1	10.3	0.91	−23.8
CTA-4	1.7	1.0	1020	1.4	300	39.8	9.4	1.23	−12.2
CTA-5	2.2	1.5	1517	1.4	341	96.1	9.4	2.15	−18.0
CTA-6	2.55	1.0	1517	1.4	148	31.1	5.2	1.13	−21.1
CTA-7	1.35	1.0	3293	1.4	186	10.6	7.3	2.87	−27.2
CTA-8	4.55	1.0	3293	1.4	96	28.9	5.4	1.43	−49.8
CTA-9	3.15	1.0	2007	1.4	110	44.2	7.3	1.21	−27.9
CTA-10	5.13	1.0	342	1.4	186	37.7	10.3	−3.00	−11.0
ST10-1	1.63	1.0	342	1.4	262	38.3	11.4	3.70	−4.38
ST10-2	3.05	1.0	1020	1.4	186	91.6	5.3	4.23	−11.3
ST10-3	2.06	1.0	1517	1.4	34.1	18.1	11.4	6.75	−9.06
ST10-4	5.1	1.0	1517	1.4	110	33.2	5.2	5.06	−17.0
ST10-5	2.7	1.0	1360	342	186	7.6	10.3	1.81	−15.8
ST10-6	4.1	1.0	1020	1.4	110	27.9	5.6	3.77	−12.8
ST10-7	2.22	1.5	683	1.4	34.1	117	4.8	6.64	−6.49

Subscript H = inlet value at high ion concentration side, subscript L = inlet value at low ion concentration side, $\dot{V}$ = pumped volume flow in the module, h = flow height in the high-concentration module.

5.2. Search for correct transport equations

Based on the experimental results presented in Table 2, the concentrations at the different material boundaries were calculated according to the theory explained in Appendices A.1–A.3. These results are shown in Table 3. The data to be fitted to the transport equations for the selective layer consists of the values c_{s3} and c_{s4} (divided by the approximated total concentration of solution $c = 55\,555$ mol/m^3) from Table 3, and, from Table 2, of the values of the pressures p_H and p_L (both expressed in Pascals and divided with $c\Re T$), the osmotic flux (changed into the molar units), and the solute flux. The reverse osmosis data of Tables 2 and 3 will be studied separately.

5.2.1. Water flux equations

A preliminary least squares (SS) estimation study for the model equations (15) and (16) suggested that the optimal values of k and n would be between 0.3–0.6 and 0.3–0.7, respectively. In this preliminary study, all parameters A_w, B_w, k and n were adjusted to the experiments. The number of adjusted parameters may be too high, when compared to the number of experiments, to make final suggestions for transport equations.

The results of the preliminary study encourage us, however, to search for a general form, applicable to all membranes to be studied, of Eqs. (15) and (16) using the rational numbers 1/3, 1/2 and 1/1 for the powers k and n. The water flux equations which were chosen for the final study and the results of the least squares estimation of these equations are reported in Table 4. Only the transport coefficients A_w, B_w and Φ are fitted to the equations. For comparison, also one-, two- and three-coefficient linear equations are studied (Eqs. (20)–(22) in Table 4). The two-coefficient equation corresponding to Eq. (21) was derived according to the linear irreversible theory of thermodynamics ([20,21]; more conventionally the osmotic- and hydrostatic pressure differences are applied as driving forces) and it is frequently used, especially in biological studies. The three-coefficient linear equation (22) can be understood as resulting, for example, in an extension to the two-coefficient linear equation (C_w is the additional transport coefficient) in cases where different partition coefficients are applied at each surface of the selective layer.

As can be seen from Table 4, the one-coefficient linear equation, Eq. (20), has a very poor correspondence to the experiments: 16 of the 24 osmosis measurements are over the 25% error limit. The two- and three-coefficient linear equations have a better but still poor fit to the results.

Overall, equations arising from the model equation (16), i.e. Eqs. (23)–(26), seem to estimate the experiments more accurately than equations arising from Eq. (15), (Eqs. (27)–(30)). Eqs. (27)–(30) result in unacceptably large errors especially in experiments where the solute concentration of the dilute side solution was

Table 3
Calculated ion concentrations at different locations (see Fig. 2)

Membrane/exp. no.	c_{s1} (mol/m^3)	c_{s2} (mol/m^3)	c_{s3} (mol/m^3)	c_{s4} (mol/m^3)
SS10-1	4.7	27.3	52.8	326.0
SS10-2	17.5	81.1	151.3	968.8
SS10-3	8.2	55.7	123.7	907.9
SS10-4	7.0	42.8	75.4	335.5
SS10-5	14.1	127.7	264	1449.0
SS10-6	362.5	523.9	685.5	1479.0
SS10-7	5.9	57.3	120.4	645.8
SS10-8	12.2	77.0	168.6	1279.6
SS10-9	8.0	24.2	31.8	172.2
CTA-1	26.4	148.3	268.4	1452.4
CTA-2	42.4	226.4	403.1	1940.1
CTA-3	389.1	594.8	811.7	1972.2
CTA-4	17.6	112.0	198.3	1000.0
CTA-5	17.8	162.6	303.5	1431.0
CTA-6	32.8	196.2	344.7	1490.1
CTA-7	67.5	303.5	544.4	3206.0
CTA-8	77.9	469.4	810.1	3222.8
CTA-9	37.0	253.3	450.8	1956.5
CTA-10	16.4	87.2	135.9	339.7
ST10-1	7.5	46.5	83.3	325.8
ST10-2	12.1	113.1	211.8	984.7
ST10-3	19.5	117.3	229.3	1313.0
ST10-4	26.7	188.3	354.7	1445.5
ST10-5	403.2	583.6	735.1	1310.4
ST10-6	21.8	136.4	245.2	978.7
ST10-7	7.0	72.2	146.4	627.1

Table 4
Transport equations for the water flux through the skin and comparison with the experimental results (SS = least squares (sum) error, >25% = number of experiments which result in a greater than 25% relative error, max. error = maximum relative error)

Model for the water flux through the selective layer		SS10			CTA			ST10		
		$SS\times10^5$ $(mol\,m^{-2}\,s^{-1})^2$	>25%	Max. error%	$SS\times10^5$ $(mol\,m^{-2}\,s^{-1})^2$	>25%	Max. error%	$SS\times10^5$ $(mol\ m^{-2}\,s^{-1})^2$	>25%	Max. error%
$A_w(\Delta x_s - \Delta p_r)$	(20)	139	6	80	12	6	75	77	4	85
$A_w\,\Delta x_s - B_w\,\Delta p_r$	(21)	90	4	90	7.3	5	40	62	3	77
$A_w x_{s4} - C_w x_{s3} - B_w\,\Delta p_r$	(22)	76	4	71	7.0	4	41	57	2	61
$A_w\,\Delta(x_s^{1/2}) - B_w\,\Delta p_r$	(23)	15	0	21	1.5	0	23	20	1	30
$A_w\,\Delta(x_s^{1/2}) - B_w\,\Delta(p_r^{1/2})$	(24)	16	0	24.8	1.2	0	18	18	1	28
$A_w\,\Delta(x_s^{1/3}) - B_w\,\Delta p_r$	(25)	15	1	75	1.7	2	33	15	1	25.2
$A_w\,\Delta(x_s^{1/3}) - B_w\,\Delta(p_r^{1/3})$	(26)	14	1	59	1.1	1	29	12	0	22
$A_w(\Delta x_s)^{1/2} - B_w\,\Delta p_r$	(27)	32	1	78	2.6	1	71	35	2	134
$A_w(\Delta x_s)^{1/2} - B_w(\Delta p_r)^{1/2}$	(28)	39	3	75	2.4	2	52	33	2	111
$A_w(\Delta x_s)^{1/3} - B_w\,\Delta p_r$	(29)	36	3	77	3.5	2	82	36	2	147
$A_w(\Delta x_s)^{1/3} - B_w(\Delta p_r)^{1/3}$	(30)	29	2	73	1.9	1	57	28	2	120
$\frac{A_w\,\Delta x_s - B_w\,\Delta p_r}{1+\Phi\bar{x}_s}$	(17)	10	0	22	0.8	0	24.8	11	1	27

increased (SS10-6, CTA-3, ST10-5) from the base level. On the other hand, the rest of the equations, Eqs. (23)–(26) and (17), mostly describe the experiments well. The SS values of these equations are close to each other. The equations with $k = 1/3$, however, result in some cases in higher relative errors than expected in the light of the repeated experiments, so we prefer the equations with $k = 1/2$ and Eq. (17). The results of the preliminary study suggested, for all membranes, a lower value than unity for n. Therefore, we prefer the model $A_w\,\Delta(x_s^{1/2}) - B_w\,\Delta(p_r^{1/2})$ compared to $A_w\,\Delta(x_s^{1/2}) - B_w\,\Delta p_r$. However, the equation $A_w\,\Delta(x_s^{1/2}) - B_w\,\Delta p_r$ should do well, at least when only the high-concentration side is pressurised. The difference between these equations should emerge if higher variations in pressure were applied than in the present study.

5.2.1.1. Effect of varying driving force in the linear water flux equation. In addition, it was verified that the accuracy of the linear water flux equations cannot be improved by replacing the molar fraction of solute with either of the following: concentration of water, molar fraction of water, concentration of solute, activity of water, osmotic potential or chemical potential of water. The last three variables of the list were calculated for a real solution, that is, the activity coefficients were accounted for. The accuracy of the linear equations does neither improve if the dimensionless pressure is replaced with the hydrostatic pressure.

5.2.1.2. Effect of varying porous support resistance and slip coefficient. We have also calculated the influence of varying the diffusion resistance of the porous support structure of the membranes and the slip coefficient of the metallic support. The effect of increasing the resistance is that the solute will concentrate more heavily inside the support structures. Lowering the slip coefficient has the same effect. The diffusion resistance was altered from 0 to an artificially high value where, due to the accumulation of solute, the molar fraction at both sides of the skin became equal. Lowering the resistance from the values reported in Table 1 had only a minute, diminishing effect to the errors produced by the non-linear equations. A minor increase in the error produced by the linear equations was noticed. The increase of the resistance from the values of Table 1 caused an increase in error of all models (the effect of varying the resistance of the SS10 membrane is illustrated in Fig. 3). However, the non-linear equations remained more accurate, except for the highest values of the resistance (approximately four times the values of Table 1), all models resulted in equal, but very poor accuracy. The effect of the slip coefficient was tested with values ranging from 0 to 0.4. No significant impact to the results was found.

5.2.1.3. Comparison with reverse osmosis tests. The reverse osmosis tests (SS10-9, CTA-10) were applied to the water flux equations (17) and (24). It was found that these equations cannot be applied for reverse osmosis, at least with the same transport coefficients. For example, test CTA-10 gives the value -1.0×10^{-7} mol/m^2 s for water flux estimated from Eq. (24), but the measured value in Table 2 is three times higher.

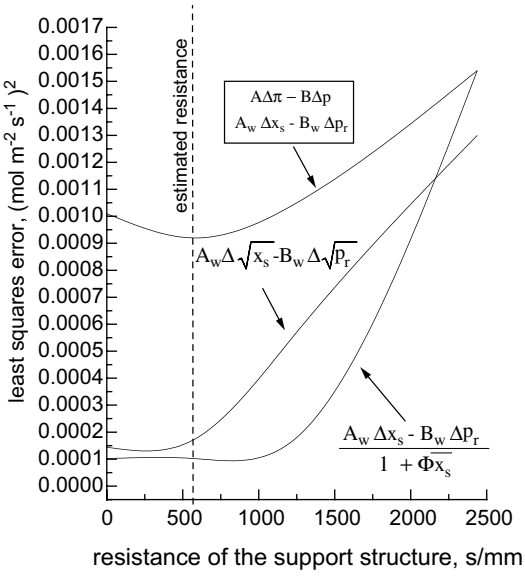

Fig. 3. Least squares error in function of the resistance of the support structure of the SS10 membrane.

5.2.2. Solute flux equations

The solute flux will be studied by optimising all the parameters (A_s, B_s, k, n) and also by setting $k = n = 1$, resulting in the one- and two-coefficient linear equations. The equations and the result of least squares optimisation of the solute flux models is shown in Table 5. The two-coefficient linear model Eq. (32) seems to fit satisfactorily to the results. Despite the increased number of optimised parameters, the models described by Eqs. (33) and (34) produced only minor improvements in accuracy compared to the two-coefficient linear equation. For the SS10 and CTA membranes, the one-coefficient linear equation, Eq. (31), gives considerably less accurate results than the two-coefficient equation and cannot be used with these membranes. For the ST10 membrane the difference is smaller.

5.3. Proposed transport equations

Eqs. (17), (24) and (32) are proposed as appropriate transport equations. The transport coefficients for the equations are reported in Tables 6 and 7. The averages of the relative errors of all the tests (disregarding the reverse osmosis tests) were, for the water flux, Eqs. (17) and (24), 11.0% and 11.8%, respectively, and for the solute flux, Eq. (32), 11.6%. These values correspond well to the variations in results found from repeated experiments.

6. Discussion

Let us consider the osmotic flow, having a velocity v_w, arising from a very simple model $J_s = c_s v_w - D_{eff}\frac{dc_s}{dy}$, which is applied in this study for the steady-state solute flow through the porous substructure. Because the solute flux is, in osmosis, considerably smaller than the solvent flux, as a first approximation we would set $J_s = c_s v_w - D_{eff}\frac{dc_s}{dy} = 0$. From this we can solve the steady-state velocity v_w created by the unequimolar flow of species. The result is a non-linear equation $v_w = D_{eff}\frac{\Delta \ln(c_s)}{\Delta y}$ in respect to the concentration difference (see also the non-linear equations, Eqs. (A.13) and (A.14), for the case $J_s \neq 0$). This is analogous to the Stefan flow arising, for example, from evaporation. If we assume that this kind of diffusion-flow phenomenon is a part of the osmotic flow process, what kind of other phenomena involved in the osmotic flow would cancel the non-linearity? Cancelling this non-linearity may, in principle, be possible; however, usually increasing complexity is more likely to cause non-linearities than linearities.

In study [10], apparent non-linear behaviour in osmotic flow was recognised for the same ST10 and SS10 membranes, as studied in this paper, when the solute concentration of the hcs was varied. This phenomenon can also be expressed by a decrease in the apparent water permeability (for increasing solute concentration difference). Similar non-linearity for various types of membranes was found in earlier experiments, for example for several different kinds of commercial membranes [11,12], for frog skin [2], for human and dog red blood cells [6], for rabbit gall-bladder [3] and for the plants *Chara australis* [8] and *Nitella translucens* [9]. While studying the osmotic transport properties of rabbit gall-bladder [3], the osmotic flux was found to

Table 5
Different forms of transport equation for the solute flux through the selective layer of the membrane and comparison with the experimental results

Model for the solute flux through the selective layer		SS10			CTA			ST10		
		SS×10^{10}	>25%	Max. error%	SS×10^{9}	>25%	Max. error%	SS×10^{9}	>25%	Max. error%
$-A_s\Delta x_s$	(31)	34	4	63	43	2	53	11	2	74
$-(A_s\Delta x_s + B_s\Delta p_r)$	(32)	4.8	0	21	4.0	0	20	6.0	1	44
$-[A_s(\Delta x_s)^{k,opt} + B_s(\Delta p_r)^{n,opt}]$	(33)	4.7	0	17	3.5	0	18	3.3	2	49
$-[A_s\Delta(x_s^{k,opt}) + B_s\Delta(p_r^{n,opt})]$	(34)	2.1	1	32	4.0	0	19	3.1	2	41

Table 6
Transport coefficients for Eqs. (24) and (32)

Membrane	$A_w \times 10^3$ (mol/m^2 s)	$B_w \times 10^3$ (mol/m^2 s)	$A_s \times 10^3$ (mol/m^2 s)	$B_s \times 10^3$ (mol/m^2 s)
SS10	605	542	2.21	17.2
CTA	134	283	5.53	98.2
ST10	561	594	4.02	37.8

Table 7
Transport coefficients for Eq. (17)

Membrane	A_w (mol/m^2 s)	Φ (dimensionless)	B_w (mol/m^2 s)
SS10	29	836	45
CTA	2.5	185	22
ST10	21	606	50

decline for a fixed concentration difference over the membrane when the average of the solute concentration across the membrane was increased. This behaviour can be seen in the proposed equations, in Eq. (17), and in Eq. (24) when transformed into the equivalent form

$$J_w = A' \frac{\Delta x_s}{\bar{x}_s^{1/2}} - B' \frac{\Delta p_r}{\bar{p}_r^{1/2}},$$

where $\bar{x}_s^{1/2}$ and $\bar{p}_r^{1/2}$ are the mean values of the square roots of the molar fraction and dimensionless pressure, respectively, and A' and B' are transport coefficients. This gives further support to the superiority of Eq. (16) (the driving force was understood to be the difference in dynamic osmotic potential) compared to the equations arising from Eq. (15) (the driving force was understood to be dependent on the concentration and pressure gradients), which cannot predict this phenomenon. Eq. (17) is actually a more general expression of the equation proposed by Diamond [3]

$$J_w = \frac{c_H - c_L}{A_w + \frac{\Phi}{2}(c_H + c_L)}$$

where c_H and c_L were bulk sucrose concentrations on both sides of the membrane. Diamond found this equation fitted well to the experiments performed with rabbit gall-bladder when the hydrostatic pressure difference was absent. The water permeability was also found, in [12], to drop with increasing solute concentration on the lcs for commercial membranes, and a non-linear effect resulting from increasing the solute concentration on the lcs was found in a study of turtle bladders [4]. As was found in [10], the water permeability of the studied SS10 and ST10 membranes also drops with increasing pressure. This has also been found previously in experiments on rabbit thoraic aorta [7].

Non-linearities in osmotic experiments are usually explained as being only apparent. It has been repeatedly assumed that when the concentration distribution of solute, especially the distribution inside the porous support structure of the membrane, is properly accounted for, the actual osmotic behaviour of the selective layer is linear. This concentration accumulation effect must be true to a certain extent, since, when the concentration of the hcs is increased, both osmotic and solute flux increase. The more the osmotic flux increases the more it prevents the solute from moving away from the structures, because the solute flux is in the opposite direction to the osmotic flux. But, as was shown in this paper, neither this internal nor the external solute distribution is able to explain, at least for the cellulose acetate membranes studied in this paper, all the non-linearity appearing in the experiments. The internal polarisation explanation is based mostly on studies [11,13]. However, we find that neither of these studies gives sufficient proof for the polarisation assumption. In study [13] an unaccountably low effective diffusion coefficient for the porous substructure (i.e. unaccountably high resistance to the solute flow) was used. The value was $D_{eff} = 4.2 \times 10^{-11}$ m^2/s, and, applying the diffusion coefficient $D = 1.5 \times 10^{-9}$ m^2/s, we get from Eq. (A.12) that the ratio between porosity and tortuosity $\varnothing/\tau$ was 0.028. The actual values of porosity and tortuosity were not reported in the article. Assuming a rather low porosity value of 0.3 for the substructure, we get an extremely high tortuosity value of $\tau = 10.7$. Furthermore, the concentration boundary layers outside the membrane were not calculated and the measured solute flux was not used to estimate the concentrations on the skin surface and the solute distribution inside the porous structure (when solute concentration distribution is estimated, the negligence of the salt flux may cause a significant error, even if the salt flux is minute compared to the water flux [22]). Only one hydrostatic pressure (difference) was used in that study. It is therefore uncertain how the linear water flux equation would have fitted to the experiments if the above facts had been properly accounted for. In Table 4 of Ref. [11] the correlation between the measured values and the predicted values was not satisfactory. While the results of the reverse osmosis experiments showed a good degree of accuracy relative to the linear water flux equation, the five osmosis experiments resulted in relative errors of 29%, 343%, 0%, 25% and 77%. The magnitude of these errors is of the same order as the inaccuracy found when the experiments described in the present paper were fitted to the linear water flow equation. In study [11] neither were the concentration boundary layers outside the membranes calculated nor the measured solute flux utilised.

As already discussed in this section, the apparent behaviour of several other types of membranes is found to be of the same kind as that of the membranes studied in this paper. Furthermore, by also taking into account the above comments about internal polarisation assumption and the results of the present analysis, the question arises of whether the osmotic non-linear

behaviour of the actual selective layer is much more general than usually supposed.

An advantage of the equation $A_w \Delta(x_s^{1/2}) - B_w \Delta(p_r^{1/2})$, in contrast to the equation $\frac{A_w \Delta x_s - B_w \Delta p_r}{1+\Phi \bar{x}_s}$, is that only two transport coefficients are needed. On the other hand, the equation $A_w \Delta(x_s^{1/2}) - B_w \Delta(p_r^{1/2})$ results, with the transport coefficients shown in Table 6, when $J_w = 0$ and simultaneously $x_{s3} = 0$, for the SS10 and ST10 membranes, in an unexpected pressure-osmotic potential relation, $\Delta p \gg \Delta\pi$ ($\approx c_s RT$). For an ideal membrane, in the case of thermodynamic equilibrium, the condition is $\Delta p = \Delta\pi$. Therefore, it is more likely to expect that, for a non-ideal membrane in a non-equilibrium situation (the membrane leaks solute when $J_w = 0$, unless $\Delta p = \Delta\pi = 0$), the condition $\Delta p \leqslant \Delta\pi$ would hold. This condition will be fulfilled when the condition $0 \ll x_{s3} < x_{s4}$ is established, which prevailed in the experiments. As these membranes have a porous substructure, where the solute concentrates more or less as a result of solute leakage, it is practically impossible to reach a situation where $x_{s3} = 0$ exists. Thus, either the equation $A_w \Delta(x_s^{1/2}) - B_w \Delta(p_r^{1/2})$ or the values of transport coefficients may reflect the appearance of the porous structure of the membrane. When $J_w = 0$, the equation $\frac{A_w \Delta x_s - B_w \Delta p_r}{1+\Phi \bar{x}_s}$ results in $\Delta p = \frac{A_w}{B_w} \Delta\pi$. As it was found that $A_w < B_w$ for all the membranes measured, we can deduce that under any conditions $\Delta p < \Delta\pi$ is fulfilled for this equation.

7. Conclusions

The osmotic flow through the cellulose acetate membranes studied cannot be estimated by applying the frequently assumed linear relationships with concentration difference, osmotic potential difference, molar fraction difference, activity difference or chemical potential difference. Several previous studies on biological and industrial membranes show similar apparent non-linear osmotic behaviour to the membranes studied in the present paper. It is commonly assumed that the non-linearities appearing in the osmosis experiments are caused by the external and, especially, the internal solute concentration distribution of the membrane substructure. There has not yet been found, however, any convincing proof supporting these assumptions. Therefore, we find it probable that the non-linear phenomenon of osmotic flow is much more general than hitherto supposed.

The proposed water transport equations are expressed as $A_w \Delta(x_s^{1/2}) - B_w \Delta(p_r^{1/2})$ and $\frac{A_w \Delta x_s - B_w \Delta p_r}{1+\Phi \bar{x}_s}$, where x_s is the molar fraction of the solute on the surface of the selective layer, p_r is the dimensionless hydrostatic pressure, and A_w, B_w and Φ are the transport coefficients. According to this study it is uncertain whether the dependence on hydrostatic pressure is linear or non-linear, although the non-linear option seems to be more likely in the two-coefficient equation.

To estimate the solute flux, the two-coefficient equation with molar fraction difference and dimensionless pressure difference as driving forces was found to be satisfactory. On the other hand, the frequently used equation in which the solute flux depends only on the concentration difference (or molar fraction difference) gave mostly poor predictions of experimental results.

It was also found that reverse osmosis behaviour in the membranes studied cannot be predicted from the suggested osmosis transport equations, when applying the same transport coefficients for both osmosis and reverse osmosis.

Acknowledgements

The authors wish to thank Professor W.J. Koros from Georgia Institute of Technology for fruitful discussions and comments on this paper and L.Sc. Kari Saari from Helsinki University of Technology for numerous pieces of advice on how to perform the experiments.

Appendix A. Estimation of the solute concentration distribution inside the fluids adjacent to the membrane, inside the metallic support and inside the porous support structure

A.1. Concentration distribution inside the channels of the module

To estimate the concentration of the solute on surfaces of the selective layer (skin), we first determine the concentration distribution inside the channels of the module. The concentration on the skin surfaces at the hcs side (c_{s4}, see Fig. 2) is received straight from the solved distribution as well as the concentration at the boundary of the lcs and the metallic support (c_{s1}). The co-ordinate system (Fig. 4) inside the channels of the module is chosen with its origin at the surface of the impermeable wall. The y-axis, which is perpendicular to the channel walls, is transformed into the dimensionless variable

$$\lambda = y/h \tag{A.1}$$

where h is the channel height.

The concentration distribution inside the channels is solved from the two-dimensional stationary state continuity equation for the solute (with constant total density of the solution)

$$u\frac{\partial c_s}{\partial x} + v\frac{\partial c_s}{h\,\partial \lambda} = D\left[\frac{\partial^2 c_s}{\partial x^2} + \frac{\partial^2 c_s}{h^2\,\partial \lambda^2}\right] \tag{A.2}$$

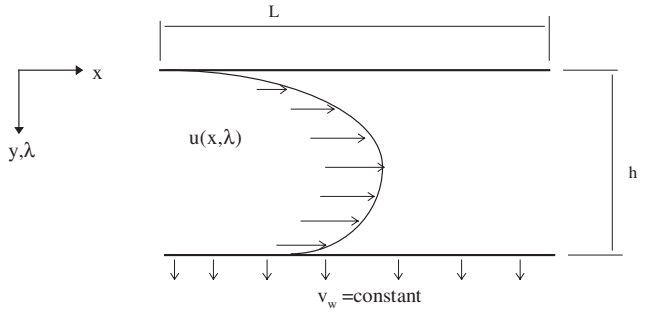

Fig. 4. Two-dimensional flow in a channel of rectangular cross-section with one permeable wall.

where $u = u(x, \lambda)$ and $v = v(x, \lambda)$ are the velocities of the solution in the x- and λ-directions, respectively, $c_s = c_s(x, \lambda)$ is the solute concentration and D is the diffusion coefficient. The boundary conditions for Eq. (A.2) are

$$c_s(0, \lambda) = \text{constant} = c_s^0 \tag{A.3}$$

$$J_s(x, 0) = 0 \tag{A.4}$$

$$J_s(x, 1) = J_s \tag{A.5}$$

where J_s is a molar solute flux through the walls of the module. At the boundary $x = L$ we use one-way coordinates, which means that the diffusion is omitted at that position. The concentration inside the channels $c_s(x, \lambda)$ is solved numerically by the control volume method from the solute-continuity equation (A.2) and the boundary conditions. The equations for u and v are presented in Appendix A.2.

A.2. Flow velocity inside a two-dimensional channel with one permeable wall

The approximate analytical solution for the velocities u and v in the case of laminar fluid flow in 2-d channel with one porous wall is, according to Seppälä [23] and Chellam et al. [24],

$$u(x, \lambda) = \left(-\frac{v_w x}{h} + u_m^0 \right) f'(\lambda) \tag{A.6}$$

$$v(\lambda) = v_w f(\lambda) \tag{A.7}$$

where f and its derivative f' can be found from the first-order perturbation approximation

$$f(\lambda) = a_{0,2}\lambda^2 + a_{0,3}\lambda^3 + Re_w \sum_{j=2}^{7} a_{1,j}\lambda^j \tag{A.8}$$

The j in λ^j denotes power and the coefficients a, which are functions of the slip coefficient of the permeable wall, are given in [23]. v_w is the velocity through the permeable wall (i.e. the osmotic flux, in this study) which is assumed to be constant.

The result is limited for sufficiently small values of wall Reynolds number (Re_w), defined as

$$Re_w = \frac{v_w h}{\nu} \tag{A.9}$$

where ν is the kinematic viscosity. The slip coefficient [17,18] is defined as

$$\Theta = \frac{k_p^{1/2}}{\alpha h} \tag{A.10}$$

where k_p is permeability of porous structure (defined by Darcy's law), α is the dimensionless constant. The permeability of the membranes was measured and the magnitude was found to be of the order of 10^{-21} m^2. As most of the flow resistance appears in the skin of the membrane, this permeability is assumed to correspond to the skin's permeability. If the magnitude of coefficient α were of the same order as the values (0.1–4) reported for different kinds of materials in [17], the slip coefficient of the skin would be practically 0. So, the membrane skin is solid-like, and the pores so small that no slip effect occurs. On the other side of the module, the metallic support has holes with diameters of 0.2 mm. Therefore, the slip effect is assumed to appear at the boundary of the metallic support and lcs. We used a value of $\Theta = 0.1$ but also calculated results when $\Theta = 0 - 0.4$.

A.3. Transport inside the metallic support and inside the porous substructure

The molar solute flux (J_s) inside the metallic support and inside the porous substructure is expressed as a one-dimensional problem:

$$J_s = c_s v_w - D_{eff} \frac{dc_s}{dy} \tag{A.11}$$

The effective diffusion coefficient D_{eff} (m^2/s) is written as

$$D_{eff} = \frac{\varnothing}{\tau} D \tag{A.12}$$

where τ and $\varnothing$ are the tortuosity and porosity of the porous matter, respectively.

Under 1-d steady-state conditions, v_w and J_s are can be considered as constants. Eq. (A.11) can be solved with boundary condition $c_s(y = 0) = c_{s1}$ and $c_s(y = \Delta y_1) = c_{s2}$ to result in

$$c_{s2} = \frac{J_s}{v_w} + \left(c_{s1} - \frac{J_s}{v_w} \right) e^{\frac{v_w}{D_{eff}} \Delta y_1} \tag{A.13}$$

where Δy_1 is the thickness of the structure.

Assuming continuity of the concentration at the boundaries of the metallic support and different porous substructure layers, we get, for the concentration after the Nth layer

$$c_{sN} = \frac{J_s}{v_w} + \left(c_{s1} - \frac{J_s}{v_w}\right) e^{v_w R_{diff}} \tag{A.14}$$

where the total resistance of diffusion (R_{diff}) is the sum of individual resistances

$$R_{diff} = \sum_{i=1}^{N} R_{diff,i} = \sum_{i=1}^{N} \frac{\Delta y_i \tau_i}{D_i \varnothing_i} \tag{A.15}$$

Applying the measured values of v_w and J_s, the calculated value of c_{s1} and the resistances given in Table 1, the concentration at the support and substructure interfaces can be estimated from Eq. (A.14).

References

[1] A. Seppälä, M.J. Lampinen, Thermodynamic optimizing of pressure-retarded osmosis power generation systems, Journal of Membrane Science 161 (1999) 115–138.

[2] Y.T. Lau, R.H. Parsons, R.J. Brady, G.A. Feeney, Water movement across split frog skin, Biochimica et Biophysica Acta 551 (1979) 448–451.

[3] J.R. Diamond, Non-linear osmosis, Journal of Physiology 183 (1966) 58–82.

[4] W.A. Brodsky, T. Schilb, Osmotic properties of isolated turtle bladder, American Journal of Physiology 208 (1965) 46–57.

[5] P.J. Bentley, Directional differences in the permeability to water of the isolated urinary bladder of the toad, *Bufo Marinus*, Journal of Endocrinology 22 (1961) 95–100.

[6] G.T. Rich, A. Sha'afi, A. Romualdez, A.K. Solomon, Effect of osmolality on the hydraulic permeability coefficient of red cells, Journal of General Physiology 52 (1966) 941–954.

[7] A. Tedgui, M.J. Lever, Filtration through damaged and undamaged rabbit thoracic aorta, American Journal of Physiology 247 (1984) H784–H791.

[8] J. Dainty, B. Hope, The water permeability of *Chara australis*, Australian Journal of Biological Sciences 79 (1964) 102–111.

[9] J. Dainty, B.Z. Ginzburg, The measurement of hydraulic conductivity (osmotic permeability to water) of internodal characean cells by means of transcellular osmosis, Biochimica et Biophysica Acta 79 (1964) 102–111.

[10] W. Ludwig, A. Seppälä, M.J. Lampinen, Experimental study of the osmotic behaviour of reverse osmosis membranes for different NaCl solutions and hydrostatic pressure differences, Experimental Thermal and Fluid Science 26 (2002) 963–969.

[11] K.L. Lee, R.W. Baker, H.K. Lonsdale, Membranes for power generation by pressure-retarded osmosis, Journal of Membrane Science 8 (1981) 141–171.

[12] G.D. Mehta, Further results on the performance on present-day osmotic membranes in various osmotic regions, Journal of Membrane Science 10 (1982) 3–19.

[13] G.D. Mehta, S. Loeb, Short-communication—internal polarisation in the porous substructures of a semi-permeable membrane under pressure-retarded osmosis, Journal of Membrane Science 4 (1978) 261–265.

[14] O. Kedem, A. Katchalsky, Permeability of composite membranes. Part 3—series array of elements, Transactions of the Faraday Society 59 (1963) 1941–1953.

[15] H.A. Massaldi, C.H. Borzi, Non-ideal phenomena in osmotic flow through selective membranes, Journal of Membrane Science 12 (1982) 87–99.

[16] P.F. Fuls, M.P. Dell, I.A. Pearson, Non-linear flow through compressible membranes and its relation to osmotic pressure, Journal of Membrane Science 66 (1992) 37–43.

[17] G.D. Beavers, D.G. Joseph, Boundary condition at a naturally permeable wall, Journal of Fluid Mechanics 30 (1) (1967) 197–207.

[18] P.G. Saffman, On the boundary condition at the surface of a porous medium, Studies in Applied Mathematics 1 (2) (1971) 93–101.

[19] H.L. Langhaar, Dimensional Analysis and Theory of Models, Robert E. Krieger Publishing Company, New York, 1980 (original edition 1951).

[20] O. Kedem, A. Katchalsky, Thermodynamical analysis of permeability of biological membranes to non-electrolytes, Biochimica et Biophysica Acta 27 (1958) 229–246.

[21] A. Katchalsky, P.F. Curran, Nonequilibrium Thermodynamics in Biophysics, Harvard University Press, Cambridge, 1965.

[22] A. Seppälä, M.J. Lampinen, M. El Haj Assad, A study on the zero flux approximation in convection–diffusion mass transfer problems, International Communications in Heat and Mass Transfer 30 (2) (2003) 207–213.

[23] A. Seppälä, Some improvements to the approximate analytical solution of the problem of laminar flow between permeable and impermeable wall, Acta Polytechnica Scandinavica, Mechanical Engineering Series 152 (2001) 1–21.

[24] S. Chellam, M.R. Wiesner, C. Dawson, Slip at a uniformly porous boundary: effect on fluid flow and mass transfer, Journal of Engineering Mathematics 26 (1992) 481–492.